# RESEARCH IN ROBUST CONTROL FOR HYPERSONIC AIRCRAFT

Progress Report #2
October 1993

1 December 1992 - 31 August 1993



Research supported by the NASA Langley Research Center
NASA Grant Number: NAG-1-1451

Principal Investigator: A.J. Calise
Research Assistant: H. Buschek
NASA Grant Monitors: J.D. McMinn
I. M. Gregory

School of Aerospace Engineering
Georgia Institute of Technology
Atlanta, Georgia 30332

# Summary

The research during the second reporting period has focused on robust control design for hypersonic vehicles. An already existing design for the Hypersonic Winged-Cone Configuration has been enhanced. Uncertainty models for the effects of propulsion system perturbations due to angle of attack variations, structural vibrations, and uncertainty in control effectiveness were developed. Using $H_\infty$ and $\mu$-synthesis techniques, various control designs were performed in order to investigate the impact of these effects on achievable robust performance.

# 1 Introduction

The objective of this research is to address the issues associated with the design of robust integrated flight control systems for future hypersonic vehicles with airbreathing propulsion systems. It is anticipated that such vehicles will exhibit significant interactions between rigid body (airframe) dynamics, structural dynamics and engine dynamics. The uncertainty in the initial dynamic models developed for these vehicles will also be high. The main reason that highly interactive uncertain dynamics are to be expected is that scramjet engines will be the primary source of propulsion at hypervelocity speeds. Wind-tunnel testing as a result will be limited, and it will be necessary to gain experience in actual flight testing of such vehicles. This means that initial flight control system design efforts will rely more heavily on theoretical and computer based models, than has been the case for subsonic and supersonic aircraft. Also, propulsion system sensitivity to angle of attack variations and structural vibrations will lead to highly interactive dynamics.

In this study, the current major research issues from a flight control viewpoint are: (1) the development of models that are representative of the interactive dynamics that can occur in such vehicles, (2) the development of representative uncertainty models for these dynamics and (3) the development of practical approaches to designing multivariable flight control systems that guarantee adequate performance in the presence of uncertainty. The research done during the second reporting period has been focusing on items (2) and (3).

The hypersonic vehicle model used in this study [1] neglects both the effects of angle of attack variations on propulsion system performance and of elastic body bending. For long, slender bodies with a considerable amount of the compression of the flow going through the engine taking place on the forebody, this assumption may not necessarily be valid for the entire flight regime. Changing the angle of attack for control purposes alters the forebody flowfield. This effect propagates through the engine and results in variations in thrust vector magnitude and direction. Low structural vibrations frequencies may lead to considerable elastic-rigid body mode interactions while flexible body bending of fore- and aftbody again affects the flowfield relevant for propulsion system performance.

In the framework of robust control design these effects are treated as uncertainties. This study has resulted in uncertainty models capturing the individual characteristics of these phenomena. The models were developed and incorporated into a control design structure which evolved from an earlier study described in Ref. [2]. A variety of robust controllers were designed utilizing $H_\infty$ and $\mu$-synthesis techniques and the sensitivity of achievable robust performance to the introduced uncertainty levels were investigated. A thorough description as well as a comprehensive discussion of the results was presented in Ref. [3] at this year's AIAA Guidance, Navigation and Control Conference in Monterey, CA, (see

Appendix). Therefore, the emphasis in this report is on a comparison of our design to the design in Ref. [2], and on additional background information not given in the paper.

# 2 Framework for the Nominal Design

The vehicle model used in this study is the Winged-Cone Configuration described in Ref. [1]. To perform control studies a five state linear model was provided by NASA Langley Research Center (courtesy of J.D. McMinn). This model was derived at an accelerated flight condition at Mach 8 with velocity, angle of attack, pitch rate, pitch attitude and altitude as state variables, and with elevon deflection and fuel equivalence ratio as control variables. The outline of our controller design structure is based on a problem formulation given in Ref. [2]. The modifications and enhancements are described in the following.

Under the assumption that normal acceleration measurements using accelerometers are easier to obtain than angle of attack measurements, $\alpha$ is replaced by the normal acceleration $n_z$ as a measurement signal which is fed back to the controller.

The time responses in angle of attack and control deflections given in Ref. [2] for an $H_\infty$-design encountering longitudinal and vertical turbulence exhibit a rather noisy behavior. In order to obtain an improved turbulence attenuation, a variety of $H_\infty$-designs with different weights (constant as well as frequency dependent) on angle of attack, pitch rate, and normal acceleration were examined. This approach turned out to be ineffective in attenuating the influence of atmospheric turbulence. It was determined that an increased penalty on the control rates $\dot{\delta e}$ and $\dot{\delta \eta}$ is effective in limiting the turbulence impact on the flight behavior of the vehicle. Accordingly, the corresponding weights were increased to

$$W_{\dot{\delta e}} = 90 \tag{1}$$

$$W_{\dot{\delta \eta}} = 50 \tag{2}$$

with respect to the weights as defined in Ref. [2]. Also in our study (see Appendix) all weights on the performance outputs are scaled in order to obtain an $\infty$-norm from disturbance inputs to performance outputs for a suboptimal $H_\infty$-controller of $\| T_{ed} \|_\infty = 0.78 < 1$. Moreover, angle of attack, pitch rate and pitch attitude were removed as performance variables.

The effect of turbulence on the system is modeled by

$$\dot{x} = Ax + Bu + B_g \begin{bmatrix} V_g \\ \alpha_g \\ q_g \end{bmatrix} \tag{3}$$

where

$$B_g = \begin{bmatrix} -a_{11} & -a_{12} & 0 \\ -a_{21} & -a_{22} & 0 \\ -a_{31} & -a_{32} & -a_{33} \\ 0 & 0 & 0 \\ 0 & 0 & 0 \end{bmatrix}. \tag{4}$$

The elements in $B_g$ are the corresponding elements of the $A$ matrix. The gust components in angle of attack and pitch rate are

$$\alpha_g = \frac{w_g}{V_0} \tag{5}$$

$$q_g = -\frac{\dot{w}_g}{V_0} = -\dot{\alpha}_g, \tag{6}$$

respectively. This turbulence model is taken from Ref. [4]. The gust terms $V_g$, $w_g$ and $\dot{w}_g$ are provided by a Dryden turbulence model. This differs from the modeling used in Ref. [2] in that the elements $a_{32}$ and $a_{33}$ in Eq. 4 are zero in the formulation in Ref. [2]. These terms represent the influence of $\alpha_g$ and $q_g$ in the pitching moment.

To illustrate the differences in the two designs a comparison of the singular values of the loop transfer function with the loop broken where velocity and altitude are fed back to the controller is shown in Fig. 1. In both cases $H_\infty$-controllers for the nominal model without uncertainty were used. It can be seen that the bandwidth of our model is reduced compared to the design in Ref. [2].

# 3 Uncertainty Modeling

The main task during the second reporting period was the development of uncertainty models representing propulsive and aeroelastic effects. A detailed description of what these models are and how they are implemented in the controller design is given in the Appendix. Some of the motivational aspects and background information is addressed below.

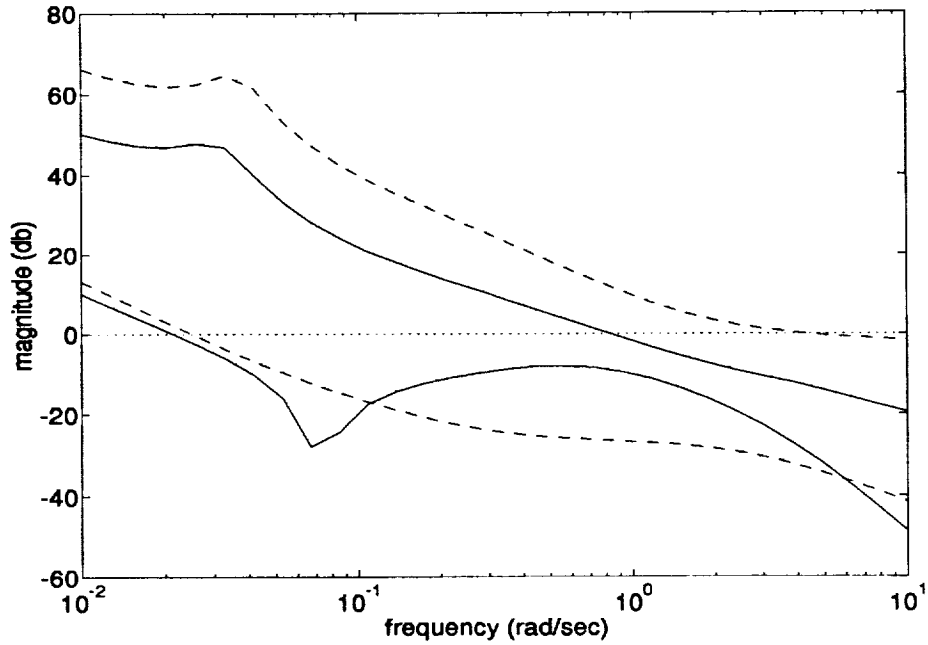


Figure 1: Comparison of singular value plots for loop broken at the V and h outputs, design in Ref. [2] (dash) vs. our design (solid).

Angle of attack changes due to vehicle control alters the flowfield along the forebody of a hypersonic vehicle. These variations in the flowfield properties propagate through the scramjet engines and affect the propulsion system performance. This results in perturbations on the thrust vector acting on the vehicle and thus influences stability and control [5]. During our first reporting period the HYTHRUST code was used to address this issue. It was observed that for the Winged-Cone Configuration the most sensitive variable to these propulsive variations was the pitching moment. At certain Mach numbers the contribution of the propulsion system to the change in the overall pitching moment was of the same order of magnitude as the aerodynamic contribution of the basic vehicle for a given angle of attack change. Hence, the pitching moment sensitivity to angle of attack variations $c_{M\alpha} = \partial c_M / \partial \alpha$ is considered the variable which will be affected the most by propulsion system perturbations. In robust control design, this effect is treated as parameter uncertainty in $c_{M\alpha}$.

Aeroelastic effects will also be of great significance when designing a flight control system for hypersonic vehicles. Elevon deflections will excite flexible modes of the configuration resulting in elastic deformations of the vehicle. Bending of fore- and aftbody again changes the flowfield properties and inflow conditions of the propulsion system leading to the effects described above. Since no aeroelastic information of the Winged-Cone Vehicle was available, a simple yet complete technique was developed to model the uncertainty

due to this effect.

The long, slender shape of the hypersonic configuration was approximated by a 2-dimensional uniform beam. The flexural deflections of such a beam are governed by the partial differential equation

$$EI\,\frac{\partial^4 y}{\partial x^4} + \bar{m}\frac{\partial^2 y}{\partial t^2} = p(x,t)\,. \tag{7}$$

The longitudinal coordinate is $x$, the vertical coordinate (deflection) is $y = f(x,t)$, $t$ is time, $E$ is the Young's modulus of elasticity, $I$ is the moment of inertia, $\bar{m}$ is the mass per unit length, and $p$ is the load per unit length and time. Using the principle of separation of variables, the general solution can be expressed by the summation of the products of the normal modes $\phi_i(x)$ multiplied by the factors $z_i(t)$

$$y(x,t) = \sum_i \phi_i(x) z_i(t) \quad i = 1, 2, \ldots\,. \tag{8}$$

The normal modes $\phi_i(x)$ are characterized by free vibration ($p(x,t) = 0$) and satisfy the differential equation

$$\frac{EI}{\bar{m}}\,\frac{\phi_i^{(iv)}(x)}{\phi_i(x)} = -\frac{\ddot{z}_i(t)}{z_i(t)} = -\omega_i^2 \tag{9}$$

which is obtained by applying the principle of separation of variables on Eq. 7. Substituting Eqs. 8 and 9 into Eq. 7, integrating over the length of the beam $L$ and observing the orthogonality property of normal modes ($\phi_n \cdot \phi_m = 0$ if $n \neq m$) yields

$$\omega_i^2 z_i(t) \int_0^L \bar{m}\,\phi_i^2(x)\,dx = \int_0^L \phi_i(x)\,p(x,t)\,dx - \ddot{z}_i(t) \int_0^L \bar{m}\,{\phi_i}^2(x)\,dx\,. \tag{10}$$

Defining modal mass as

$$M_i = \int_0^L \bar{m}\,\phi_i^2(x)\,dx \tag{11}$$

and modal force as

$$F_i = \int_0^L \phi_i\,p(x,t)\,dx\,, \tag{12}$$

Eq. 10 can be written as

$$M_i\,\ddot{z}_i(t) + \omega_i^2\,M_i\,z_i(t) = F_i(t)\,, \quad i = 1, 2, \ldots \tag{13}$$

Introducing modal damping by simply adding the damping term gives

$$\ddot{z}(t) + 2\,\zeta_i\,\omega_i \dot{z}_i(t) + \omega_i^2\,z_i(t) = \frac{F_i(t)}{M_i}\,. \tag{14}$$

Since the elastic vibrations are caused by elevon deflections the force acting on the body is the lift increment at the elevon location:

$$p(x,t) = P(t) \text{ at } x = x_p \,. \tag{15}$$

So the modal force simplifies to

$$F_i(t) = P(t)\,\phi_i(x_p)\,. \tag{16}$$

If we further replace the deflection $y(x,t)$ by the deflection angle $\theta(x,t)$ using

$$\theta(x,t) \approx \tan\theta(x,t) = \frac{\partial y(x,t)}{\partial x} \tag{17}$$

and the principle of seperation of variables, we obtain

$$\theta_i(x,t) = \frac{\partial}{\partial x}[\phi_i(x)\,z_i(t)] = \frac{d\phi_i(x)}{dx}\,z_i(t)\,. \tag{18}$$

Substituting Eqs. 16 and 18 into Eq. 14 and applying the Laplace transform yields a second order transfer function from the elevon lift force $P(s)$ to the body deflection angle $\theta(x,s)$ in terms of the elastic characteristics of the body:

$$\theta_i(x,s) = \frac{\phi_i(x_p)\,\dfrac{d\phi_i(x)}{dx}}{(s^2 + 2\zeta_i\omega_i s + \omega_i^2)\,M_i}\,P(s) \tag{19}$$

where $i$ accounts for the individual modes. The implementation of this transfer function into the controller design as an uncertainty model is described in the Appendix.

The natural frequencies of a hypersonic configuration will most likely be uncertain to begin with. Additionally, aerodynamic heating during high speed atmospheric flight will affect the elastic characteristics of the vehicle. Increased heating loads tend to decrease the natural frequencies of the flexible modes. The transfer function in Eq. 19 possesses the property that for decreasing natural frequencies, the peak value of its frequency response increases. The frequency response for two different sets of natural frequencies is shown in Fig. 2. As the elastic mode frequencies approach the rigid body frequencies, the level of uncertainty increases.

Uncertainty in the control effectiveness was already addressed in Ref. [2]. There, constant levels of uncertainty were inserted simultaneously in both control channels. In our study we extend this approach to frequency dependent uncertainty models to account for increasing uncertainty with increasing frequency at the plant input. The uncertainty weight was chosen to be

$$W_{\Delta act} = \frac{k_{act}(s+10)}{s+1000} \tag{20}$$

where $k_{act}$ determines the uncertainty level for low frequencies. This weighting function is illustrated in Fig. 3.

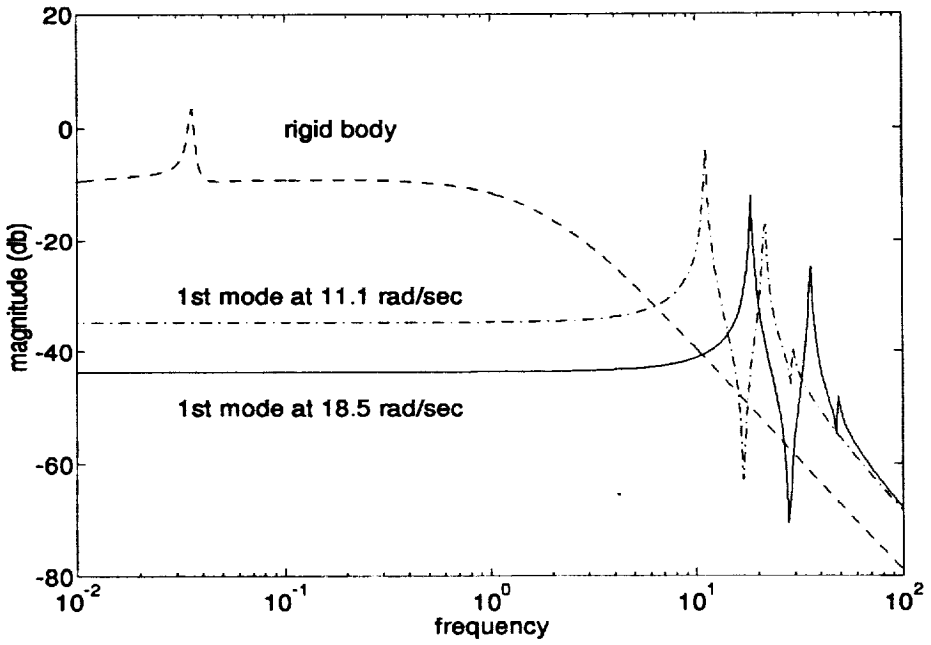


Figure 2: Deflection angle responses to elevon input.

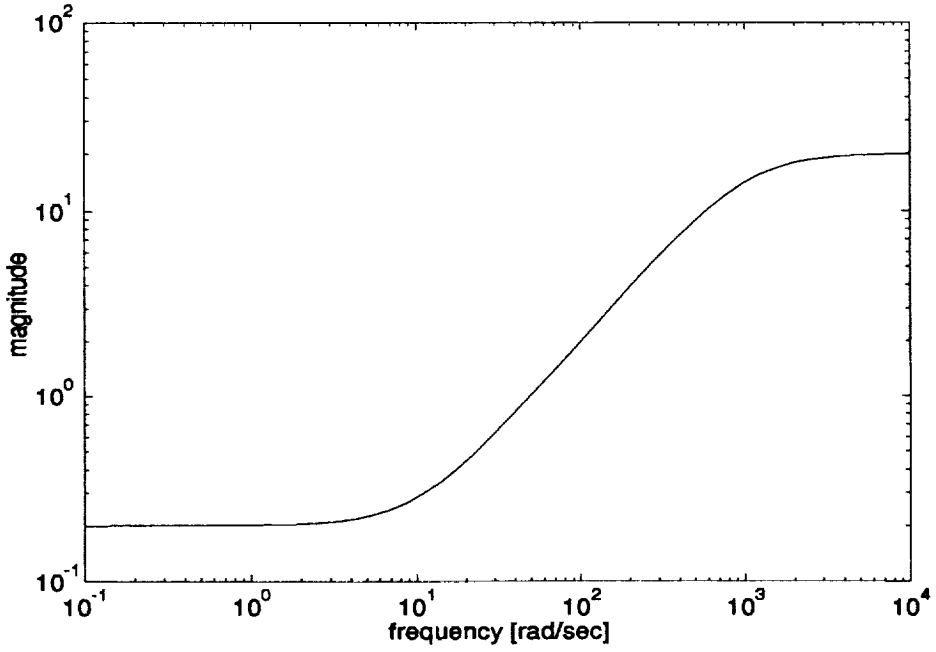


Figure 3: Weighting function for uncertainty in control effectiveness, $k_{act} = 20$.

# 4 Results and Conclusions

A complete discussion of the robust control design procedure and the results is given in the Appendix. The main conclusions are summarized below:

- The design for robust performance with all uncertainties modeled simultaneously demonstrates that $H_\infty$ and $\mu$ analysis and synthesis methods are ideal for addressing multiple uncertainty sources in hypersonic flight control design.
- Flexible fuselage bending and control effectiveness has a greater impact on achievable robust performance in comparison to uncertainty due to propulsion system variations. To a certain extend, this confirms the observations made with the HYTHRUST code during our first reporting period [5].
- Mutual coupling effects among the individual phenomena decrease the admissible uncertainty levels for which robust performance is achievable. This shows that sophisticated uncertainty modeling with reduced conservatism will be crucial for a successful flight control design for hypersonic vehicles.
- The controllers obtained using $\mu$-synthesis techniques are usually of rather high order. An attempt to reduce the order of the controller using various model reduction techniques failed in that robust performance was lost for the system using the reduced order controllers. This shows the need to employ fixed order controller design techniques.

# 5 Future Research

Based on the results from our first year's research the focus of our future work will be on three major topics:

1. Fixed order controller design methodology will be developed and applied on the hypersonic vehicle model investigated in this report. First steps have already been taken to extend the fixed order $H_\infty$ design described in Ref. [6] to a $\mu$-synthesis framework and encouraging results were obtained for a simple example.
2. Atmospheric turbulence has a significant impact on the level of control activity in hypersonic flight. A possibility to attenuate this influence is to impose an additional $H_2$ constraint. This will be done in the differential game setting for fixed order $H_\infty$ control described in Refs. [6] and [7]. This is the so-called mixed $H_2/H_\infty$ problem for which no complete solution presently exists even in the full order case.

3. To further reduce conservatism in the uncertainty modeling, the issue of real parameter uncertainty will be investigated. $\mu$-synthesis accounts for structure in the uncertainty but treats real parameters as complex which is overly conservative. Again, the differential game formulation can be employed to treat uncertain parameter variations (in addition to external disturbances) as an opponent trying to maximize the performance index while the controller tries to minimize the same performance index. Another approach to solve the real $\mu$ problem that is currently under development is the mixed $\mu$-analysis using the so-called G-scales in addition to the D-scales which is described in Refs. [8] and [9]. Also, results have already been obtained by treating the uncertainty as nonlinearity and applying techniques from Absolute Stability Theory such as the Popov Criterion, e.g. see Ref. [10]. We will look into these different approaches as well as possible combinations in order to solve the problem of real/mixed $\mu$-synthesis.

# References


[1] J.D. Shaughnessy et al. "Hypersonic Vehicle Simulation Model: Winged-Cone Configuration". NASA TM 102610, November 1990.

[2] I.M. Gregory et al. "Hypersonic Vehicle Control Law Development Using $H_\infty$ and $\mu$-Synthesis". In *Proceedings of the $4^{th}$ AIAA International Aerospace Planes Conference*, Orlando, FL, December 1992.

[3] H. Buschek and A.J. Calise. "Robust Control of Hypersonic Vehicles Considering Propulsive and Aeroelastic Effects". In *Proceedings of the 1993 AIAA Guidance, Navigation and Control Conference*, Monterey, CA, August 1993.

[4] R.C. Nelson. *Flight Stability and Automatic Control.* McGraw-Hill, New York, 1989.

[5] A.J. Calise and H. Buschek. "Research in Robust Control for Hypersonic Vehicles". Progress Report No. 1 to NASA Langley Research Center, Contract No. NAG-1-1451, November 1992.

[6] G.D. Sweriduk and A.J. Calise. "Robust Fixed Order Dynamic Compensation: A Differential Game Approach". In *Proceedings of the 1993 IEEE Conference on Aerospace Control Systems*, West Lake Village, CA, May 1993.

[7] A.J. Calise. "$H_2$ and $H_\infty$ Formulations for Fixed Order Dynamic Compensator Design". Plenary Talk for the *IEEE Conference on Aerospace Control Systems*, West Lake Village, CA, May 1993.

[8] M.K. Fan, A.L. Tits, and J.C. Doyle. "Robustness in the Presence of Mixed Parametric Uncertainty and Unmodeled Dynamics". *IEEE Transactions on Automatic Control*, Vol. 36, No. 1, pp. 25-38, January 1991.

[9] P.M. Young, M.P. Newlin, and J.C. Doyle. "$\mu$ Analysis with Real Parametric Uncertainty". In *Proceedings of the $30^{th}$ Conference on Decision and Control*, Brighton, England, December 1991.

[10] W.M. Haddad and D.S. Bernstein. "Parameter-Dependent Lyapunov Functions and the Popov Criterion in Robust Analysis and Synthesis". Submitted to *IEEE Transactions on Automatic Control.*

# Appendix

1115

# ROBUST CONTROL OF HYPERSONIC VEHICLES CONSIDERING PROPULSIVE AND AEROELASTIC EFFECTS

Harald Buschek* and Anthony J. Calise**
Georgia Institute of Technology
Aerospace Engineering
Atlanta, GA

**Abstract**

The influence of propulsion system variations and elastic fuselage behavior on the flight control system of an airbreathing hypersonic vehicle is investigated. Thrust vector magnitude and direction changes due to angle of attack variations affect the pitching moment. Low structural vibration frequencies may occur close to the rigid body modes influencing the angle of attack and lead to possible cross coupling. These effects are modeled as uncertainties in the context of a robust control study of a hypersonic vehicle model accelerating through Mach 8 using $H_\infty$ and $\mu$ synthesis techniques. Various levels of uncertainty are introduced into the system. Both individual and simultaneous appearance of uncertainty are considered. The results indicate that the chosen design technique is suitable for this kind of problem provided that a fairly good knowledge of the effects mentioned above is available. The order of the designed controller is reduced but robust performance is lost which shows the need for fixed order design techniques.

## 1. Introduction

Hypersonic atmospheric flight will be one of the most challenging efforts undertaken by aerospace scientists at the end of this century. Aerospace vehicles have to perform in speed ranges from subsonic to hypersonic up to Mach 25, and therefore will encounter a variety of effects that have not been addressed before in the development of one single vehicle. One of the most crucial aspects will be a strong interaction between aerodynamics, structure, and propulsion system and their impact on performance, guidance and control characteristics [1].

In hypersonic propulsion, unlike present subsonic/supersonic engines, the entire vehicle aerodynamic configuration must be considered as part of the propulsion system. Before reaching the inlet the external flow will be compressed along the forebody, and after leaving the combustor the aftbody is utilized as an external nozzle. Changing the angle of attack for control purposes alters these flow fields and results in variations in thrust vector magnitude and direction influencing stability and control of the vehicle. The most sensitive quantity in this respect is the pitching moment [2], the control of which is vital to stabilize typically long and slender bodies of aerospace vehicles at this speed regime.

The need for a low structural weight mass fraction introduces relatively low structural vibration frequencies. Significant elastic-rigid body mode interactions are likely to occur imposing additional requirements on the flight control system. Additionally, bending of the forebody influences the flow conditions at the inlet which propagates through the engine and together with the elastic deformation of the aftbody again affects the thrust vector [3]. Determination of the elastic mode shapes will be highly uncertain.

These features, among others, illustrate the necessity of designing a robust, highly integrated flight control system for future hypersonic vehicles with airbreathing propulsion systems. In this paper, uncertainty models are developed to address the two major effects mentioned above, and, together with additional uncertainty on the control effectiveness, their impact on achievable robust performance is investigated. This is done within the context of a flight control system design using $\mu$-synthesis design techniques. The uncertainty modeling is described, and a sensitivity study of achievable robust performance to the uncertainty level is carried out. In an additional design step the order of the obtained controller is reduced using several different methods, and a comparison with the full order design is presented.

## 2. Brief Review of $\mu$-Synthesis

This section provides a concise summary of the general framework of $\mu$-synthesis in order to define the terminology used in the paper. A thorough discussion on $H_\infty$ and $\mu$ control theory is provided in Refs. [4]-[6].

The framework for robust control design is illustrated in Fig. 1. $P$ is the generalized plant, $K$ denotes the controller, and $\Delta$ represents the uncertainties on the system due to parameter variations, unmodeled dynamics, nonlinearities and various assumptions. The input vector, $d$, denotes all external

*Graduate Research Assistant, Student Member AIAA
**Professor, Fellow, AIAA

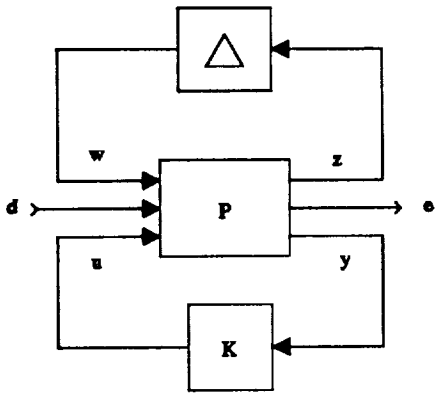


Figure 1: Framework for robust control design.

disturbances acting on the plant, such as commands, disturbances and sensor noise. The output vector $e$ contains the regulated performance variables. Feedback measurements are denoted by the vector $y$, and $u$ represents the control vector that is the input to the plant actuators. The inputs and outputs corresponding to the uncertainties in the system are $w$ and $z$, respectively. The input disturbances and uncertainties are normalized to unity bounds by constant or frequency dependent weights, which are incorporated into the generalized plant, $P$. The uncertainty $\Delta$ is considered to be complex with a block diagonal structure consisting of $s$ scalar blocks and $f$ full blocks

$$\Delta = \mathrm{diag}\{\delta_1 I_{r1} \ldots \delta_s I_{rs}, \Delta_1 \ldots \Delta_f\} \tag{1}$$

where

$$\delta_i \in \mathbf{C}, \Delta_j \in \mathbf{C}^{mj \times mj}. \tag{2}$$

The bounded set $\mathbf{\Delta}_\delta$ is defined as

$$\begin{aligned} \mathbf{\Delta}_\delta &= \{\Delta: |\delta_i| \leq \delta, \bar{\sigma}(\Delta_j) \leq \delta\} \\ &= \{\Delta: \bar{\sigma}(\Delta) \leq \delta\} \end{aligned} \tag{3}$$

If the controller is wrapped into the plant $P$, the resulting system $M$ is defined by the lower *Linear Fractional Transformation*

$$\begin{aligned} M &= F_l(P, K) \\ &= P_{11} + P_{12}K(I - P_{22}K)^{-1}P_{21} \end{aligned} \tag{4}$$

This defines the analysis structure which is shown in Fig. 2. It is assumed that $M$ is stable.

To account for the structure in the uncertainty $\Delta$, the *Structured Singular Value* $\mu(M_{11})$ is introduced which is defined by

$$\mu(M_{11}) = \begin{cases} \left\{\min_{\Delta \in \mathbf{\Delta}_\infty} [\bar{\sigma}(\Delta): \det(I - M_{11}\Delta) = 0]\right\}^{-1} \\ 0 \text{ if } \det(I - M_{11}\Delta) \neq 0, \forall \Delta \in \mathbf{\Delta}_\infty. \end{cases} \tag{5}$$

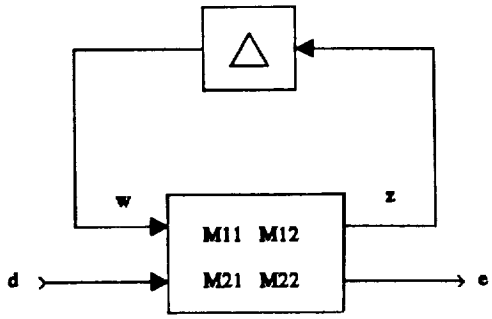


Figure 2: Analysis structure.

The corresponding $\mu$-measure is

$$\|M_{11}\|_\mu = \sup_\omega \mu(M_{11}) \tag{6}$$

Note that the $\mu$-measure is not a norm and depends both on $M$ and the structure of $\Delta$.

With these preliminaries stated the concepts of performance, stability, and robustness can now be addressed. Referring to Fig. 2, in $\mu$-synthesis the performance output $e$ is scaled so that nominal performance ($NP$) is said to be satisfied if the disturbance attenuation condition

$$\|M_{22}\|_\infty < 1 \tag{7}$$

is satisfied. In Eq. (7) the $\mathrm{H}_\infty$-norm is defined as

$$\|M_{22}\|_\infty = \sup_\omega \bar{\sigma}\left(M_{22}(i\omega)\right). \tag{8}$$

Robust stability ($RS$) is satisfied if and only if (iff)

$$\|M_{11}\|_\mu < 1, \Delta \in \mathbf{\Delta}_1. \tag{9}$$

For unstructured uncertainty, the $\mu$-measure equals the $\mathrm{H}_\infty$-norm.

The robust performance problem is converted into an equivalent robust stability problem by augmenting the uncertainty block with a fictitious full uncertainty block $\Delta_p$ as shown in Fig. 3. With this formulation, robust performance ($RP$) is satisfied iff

$$\|M\|_\mu < 1, \Delta_{aug} \in \mathbf{\Delta}_1. \tag{10}$$

where $\Delta_{aug}$ stands for the augmented uncertainty.

The Structured Singular Value cannot be calculated directly. An upper bound can be computed from:

$$\mu(M) \leq \inf_{\mathbf{D}} \bar{\sigma}(DMD^{-1}) \tag{11}$$

where $D = \mathrm{diag}\{d_i I_i\}$ with the same dimensional structure as $\Delta$. The equality on this upper bound holds in some cases, but is not true in general. However, the optimization problem for the upper bound is

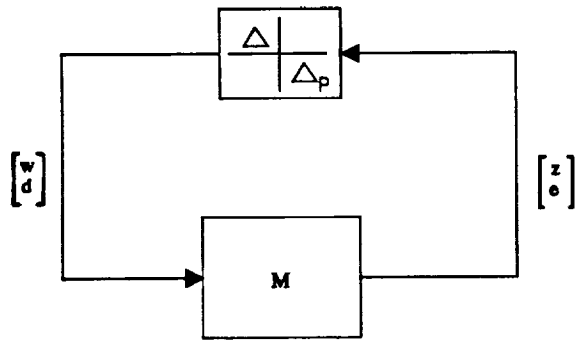


Figure 3: Structure for addressing robust performance.

convex leading to an upper bound value that is fairly close to the $\mu$ value in most cases. The robust performance test can be expressed in terms of this upper bound:

$$\inf_{D} \|DMD^{-1}\|_\infty < 1 \Rightarrow \text{RP}. \tag{12}$$

Note that it has become an $\infty$-norm test.

$H_\infty$-design and $\mu$-analysis are combined to perform $\mu$-synthesis. Recalling Eq. (4), an optimal controller can be achieved by solving the optimization problem

$$\inf_{K,D} \|DF_l(P,K)D^{-1}\|_\infty \tag{13}$$

Presently, it is not known how to solve this minimization. An approximation to $\mu$-synthesis involves a sequence of minimizations, first over the controller variable $K$ (holding the $D$ variable fixed), and then over the $D$ variable (holding the $K$ variable fixed). This is often referred to as the *D-K iteration*.

### 3. Hypersonic Vehicle Model

The hypersonic vehicle model used in this study is the Winged-Cone Configuration described in Ref. [7]. Main characteristics of this vehicle are an axisymmetric conical forebody, a cylindrical engine nacelle section with engine modules all around the body, and a cone frustrum engine nozzle section. In order to carry out control studies, a five state linear model of the longitudinal dynamics is used representing flight conditions for an accelerated flight through Mach 8 at approximately 86000 ft (see Appendix). State and control variables are:

$$\mathbf{x} = \begin{bmatrix} V \\ \alpha \\ q \\ \theta \\ h \end{bmatrix} = \begin{bmatrix} \text{velocity (ft/sec)} \\ \text{angle of attack (deg)} \\ \text{pitch rate (deg/sec)} \\ \text{pitch attitude (deg)} \\ \text{altitude (ft)} \end{bmatrix} \tag{14}$$

$$\mathbf{u} = \begin{bmatrix} \delta e \\ \delta \eta \end{bmatrix} = \begin{bmatrix} \text{symmetric elevon (deg)} \\ \text{fuel equivalence ratio (-)} \end{bmatrix} \tag{15}$$

Since the linear model is obtained at a non-equilibrium flight condition where the vehicle acceleration is non-zero, it should be noted that the state and control variables are perturbation quantities representing deviations from a climbing and accelerating flight condition. This model represents pure rigid body dynamics and therefore does not account for any aeroelastic effects. Also, the propulsion system model used for the Winged-Cone Configuration does not include sensitivity to angle of attack variations. On the other hand, these effects are considered crucial for vehicle stability and control and will be treated in this paper as uncertainty.

The interconnection structure for the controller design used in this study is shown in Fig. 4 and has been derived from the design in Ref. [8]. Velocity, altitude, normal acceleration, pitch rate, and pitch attitude are the fedback variables. Normal acceleration is determined by

$$n_z = \frac{V_0}{57.3g}(\dot{\alpha} - q) \tag{16}$$

where $V_0$ is the velocity at the flight condition for which the linear model was obtained, 57.3 is the conversion from radians to degrees, and $g$ is acceleration due to gravity. Control actuator dynamics are represented by first order filters with 30 rad/sec bandwidth for elevon and 100 rad/sec bandwidth for fuel equivalence ratio. The design is carried out as a velocity and altitude command tracking system. Additional disturbances include Dryden turbulence models and sensor noise.

The turbulence spectrum is defined by the weights

$$F_u(s) = \sqrt{\frac{2V_0\sigma_u^2}{L_u}}\,\frac{1}{s + V_0/L_u} \tag{17}$$

for longitudinal and

$$F_w(s) = \sqrt{\frac{3V_0\sigma_w^2}{L_w}}\,\frac{s + V_0/(\sqrt{3}L_w)}{(s + V_0/L_w)^2} \tag{18}$$

for vertical wind gusts [9]. For the reference altitude used in this study [10]

$$\sigma_u = 10.8\,\text{ft/sec},\ \sigma_w = 6.88\,\text{ft/sec}, \tag{19}$$

$$L_u = 65574\,\text{ft},\ L_w = 26229\,\text{ft}. \tag{20}$$

Turbulence introduces the gust quantities $V_g$, $\alpha_g$ and $\dot{\alpha}_g$ into the system (see Fig. 4 and Appendix). A measurement weight

$$W_{noise} = 10^{-6}\,\mathrm{I}_5 \tag{21}$$

is imposed on the fedback variables.

The weighting functions on velocity and altitude error reflect specific performance requirements and were

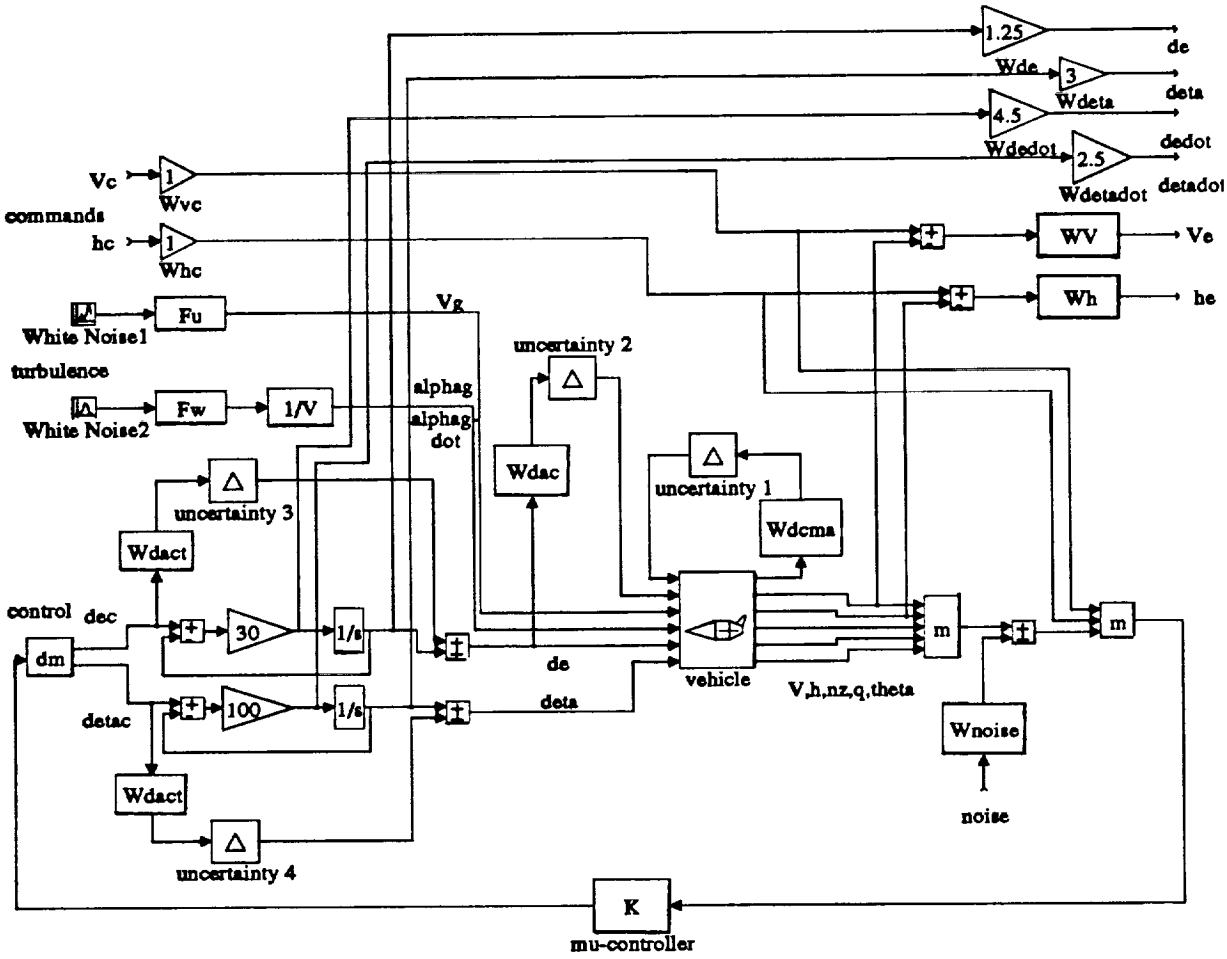


Figure 4: Interconnection structure for controller design.

derived in Ref. [8] from a near fuel optimum ascent trajectory for this vehicle. The weighting on the velocity and altitude errors are

$$W_V = \frac{2.5 \cdot 10^{-2}(s + 4.33 \cdot 10^{-2})}{s + 4.33 \cdot 10^{-5}} \tag{22}$$

and

$$W_h = \frac{2.5 \cdot 10^{-2}(s + 4.95 \cdot 10^{-2})}{s + 4.95 \cdot 10^{-5}} \tag{23}$$

and allow for 10% overshoot and 5% steady state error in the time responses of each velocity and altitude. Control deflections and control rates are the only other weighted performance outputs. The control deflection weights are chosen to be

$$W_{\delta e} = 1.25 \tag{24}$$

$$W_{\delta \eta} = 3. \tag{25}$$

In order to reduce the sensitivity of the control response to atmospheric disturbances the weights on the actuator rates are selected to be

$$W_{\dot{\delta} e} = 4.5 \tag{26}$$

$$W_{\dot{\delta} \eta} = 2.5. \tag{27}$$

The uncertainties appearing at various locations in the diagram in Fig. 4 will be addressed in the following section.

## 4. Uncertainty Modeling

Aerospace vehicles in hypersonic flight regimes will typically utilize scramjet propulsion systems which are highly integrated into the airframe. This results in an increased sensitivity to variations in angle of attack [11]. The most important impact of these propulsive perturbations is on the pitching moment leading to significant control surface deflections to stabilize the vehicle [2]. This phenomenon is addressed as parametric uncertainty in the pitching moment sensitivity to angle of attack variations, $c_{M\alpha}$. The uncertainty is represented by a scalar perturbation to the nominal model. This perturbation can be rearranged to obtain input and output quantities $w_\Delta$ and $z_\Delta$. $\Delta$ in this case is a scalar since only one parameter is perturbed. The matrices $B_\Delta$, $C_\Delta$, and $D_\Delta$ can be chosen

from the uncertain model

$$\begin{aligned} \dot{x} &= Ax + B_\Delta w_\Delta + Bu \\ z_\Delta &= C_\Delta x + D_\Delta u \\ y &= Cx + Du \\ w_\Delta &= \Delta z_\Delta \end{aligned} \tag{28}$$

If a scaling has been applied so that the values of $\Delta$ range between -1 and 1, Eq. (28) represents the set of all possible models. For the case of uncertainty in the parameter $c_{M\alpha}$ which occurs in the (3,2) element of the A matrix, the uncertainty matrices are

$$B_\Delta = [0\,0\,1\,0\,0]^T \tag{29}$$

$$C_\Delta = [0\,1\,0\,0\,0] \tag{30}$$

$$D_\Delta = 0 \tag{31}$$

It should be noted that this approach leads to a conservative representation since it also permits complex perturbations in real aerodynamic coefficients. This uncertainty is labeled "uncertainty 1" in Fig. 4.

Significant coupling between the elastic and rigid body modes is expected for this vehicle type which has to be considereed in the design of a flight control system. Moreover, fuselage bending affects propulsion system performance which in turn influences the rigid body flight dynamics or even excites the elastic modes [3]. Since the model used in this study comprises only rigid body dynamics and no aeroelastic information on the Winged-Cone Accelerator was available a simple yet concise method had to be developed to introduce aeroelastic effects as uncertainty into the rigid body behavior.

A second order transfer function was derived exhibiting elastic deformations of a long, slender, uniform body caused by a force $P(s)$ suddenly applied at a certain location of the body, $x_p$ [12]:

$$\theta_i(x,s) = \frac{\phi_i(x_p)\,\frac{d\phi_i(x)}{dx}}{(s^2 + 2\zeta_i\omega_i s + \omega_i^2)\,M_i}\,P(s) \tag{32}$$

$\theta_i(x,s)$ is the angle by which the deformed body is deflected from its original shape due to the $i^{th}$ elastic mode, $\phi_i(x)$ is the mode shape function of the $i^{th}$ elastic mode, $\zeta_i$ and $\omega_i$ are the corresponding damping ratio and natural frequency, respectively, and $M_i$ is the modal mass defined by

$$M_i = \int_0^L m(x)\,\phi_i^2(x)\,dx \tag{33}$$

where $m(x)$ is the mass distribution and $L$ the length of the body. In the case of the Winged Cone Vehicle structural excitement is caused by lift increments due to elevon deflections:

$$\begin{aligned} P(s) &= \delta L(s) \\ &= 2\frac{\partial c_{L,da}}{\partial \delta e}\,q\,S_{ref}\,\delta e(s) \end{aligned} \tag{34}$$

where $q$ is the dynamic pressure for the given flight condition, $S_{ref}$ the reference area, and $\partial c_{L,da}/\partial \delta e$ the sensitivity of the lift coefficient of one elevon to the elevon deflection. This was graphically determined from Ref. [7]. The body deflection angle $\theta(x,s)$ can also be interpreted as change in the angle of attack $\Delta\alpha(x,s)$ due to elastic deformation. As mentioned above, angle of attack perturbations affect the rigid body dynamics via the propulsion system, thus the transfer function given in Eq. (32) is evaluated at the location of the inlet entrance. The resulting estimation of the angle of attack variation due to flexible body motion excited by elevon deflections is then fed as uncertainty into the rigid body model, using the second column of the nominal plant A matrix (see Fig. 4 and Eq. (14)).

Unfortunately, no information on the mode shapes $\phi_i(x)$ of the Winged-Cone Accelerator was available for this study. So the rather crude assumption of a uniform beam with both ends free was chosen to model the elastic mode shapes. The analytical solution to this problem can be found in any textbook on structural dynamics (e.g. [12]). The natural frequencies are taken from a generic NASP configuration investigated in Ref. [13]. The first three fuselage bending modes of the unheated vehicle are considered and are given by $\omega_1 = 2.95$ Hz, $\omega_2 = 5.72$ Hz, and $\omega_3 = 7.74$ Hz. The damping ratio for structural vibration modes is typically small and was chosen to be $\zeta_i = 0.01$ for all three frequencies. The frequency response of the resulting flexible mode function in Eq. (32) is shown in Fig. 5. Due to the "uniform beam" approximation an amplification was necessary to achieve a reasonable response magnitude which in this case translates into 0.25° peak uncertainty in $\alpha$ for a 1° sinusoidal variation in elevon at $\omega = \omega_1$. Also given in Fig. 5 is the response of the rigid body due to elevon deflections and a cover function which was used for the controller design. The cover function is given by

$$W_{\Delta\alpha,c} = \frac{k_c\,(s+2)}{s^2 + 2\zeta_c\omega_c s + \omega_c^2} \tag{35}$$

with $k_c = 2.5$, $\zeta_c = 0.25$ and $\omega_c = 19.53$ rad/sec.

The effect of aerodynamic heating during high-speed flight through the atmosphere on the elastic characteristics of a hypersonic vehicle was addressed in Ref. [13]. One conclusion was that for increasing aerothermal heating loads (related to increasing Mach numbers) the natural frequencies of the fuselage bending modes decreased. This envokes the potential of rigid/elastic body mode coupling. Although the longitudinal model used in the present study accounts only for one Mach number, this effect will be considered by letting the frequencies of the elastic modes vary from 100% to 60% of their values for the unheated vehicle. The cover function used for the controller design was fitted accordingly by adjusting the parameters from

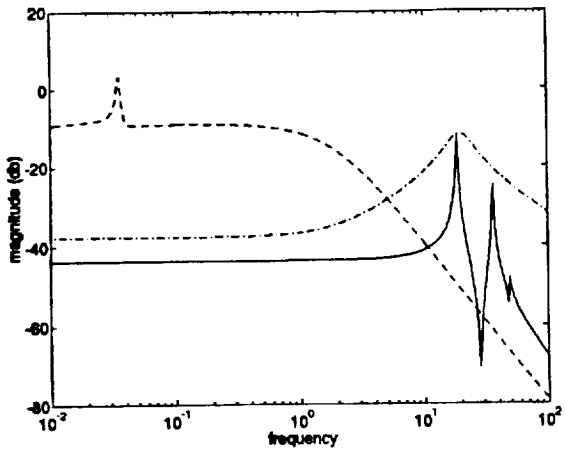


Figure 5: Angle of attack responses to elevon input: flexible body approximation (solid), rigid body (dash), and cover function (dash dot)

Eq. (35). One feature of the elastic mode approximation used in this study is the fact that for decreasing frequencies the peak value of its frequency response increases. Thus, the closer the elastic modes get to the rigid body frequencies, the more uncertainty in the angle of attack is inserted into the system. This uncertainty is labeled "uncertainty 2" in Fig. 4.

The third type of uncertainty introduced into the system is uncertainty on the control effectiveness in both elevon and equivalence ratio control channels, depicted "uncertainty 3" and "4" in Fig. 4. The uncertainties are represented multiplicatively around the actuators and occur simultaneously. This issue was already addressed in Ref. [8] using constant levels of uncertainty, here, the uncertainty weight on each channel is modeled as

$$W_{\Delta act} = \frac{k_{act}(s+10)}{s+1000} \tag{36}$$

to account for increasing uncertainty with increasing frequency at the plant input. $k_{act}$ determines the uncertainty level for low frequencies.

### 5. Preliminary Sensitivity Studies

Before analyzing the impact of the various uncertainties introduced in the previous section on the achievable robust performance, an $H_\infty$-controller for the nominal model without any uncertainty is designed in order to scale nominal performance. The $\infty$-norm from disturbances to errors disregarding uncertainty for the closed loop system was $||T_{ed}||_\infty = 0.78$.

In a first series of investigations only the effect of parameter uncertainty in $c_{M\alpha}$ was addressed. For a variety of uncertainty levels an $H_\infty$-controller was designed and a series of succesive D-K iterations lead to the final $\mu$-controller. Fig. 6 shows the curves for the upper bound on the $\mu$ values representing robust performance bounds of the system for designs with 25%, 50%, 75%, and 100% uncertainty in the aerodynamic coefficient $c_{M\alpha}$. The values of the $\mu$ bounds do not exceed 1 implying that robust performance is achievable even for 100% uncertainty in $c_{M\alpha}$.

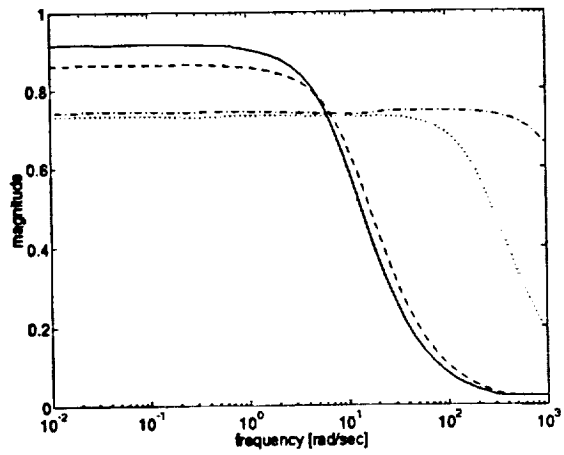


Figure 6: Robust performance bounds for 25% (dot), 50% (dash dot), 75% (dash), and 100% (solid) uncertainty in $c_{M\alpha}$.

Similar to the $c_{M\alpha}$ uncertainty study, investigations with respect to the angle of attack uncertainty due to fuselage bending were carried out. As discussed in the previous section, the frequency range over which the flexible modes occur is varied to account for aerodynamic heating effects. Robust performance bounds for angle of attack uncertainties specified in Table 1 are shown in Fig. 7. Again, robust performance was achievable in all cases. However, the results indicate that achievable robust performance is very sensitive to the frequency of the first flexible mode.

The last uncertainty representation to be analyzed is the simultaneously occuring uncertainty in the actuators. Low frequency uncertainty levels of 10%, 20% and 30% were imposed on the control effectiveness. The corresponding robust performance bounds are depicted in Fig. 8. Note that robust performance is not

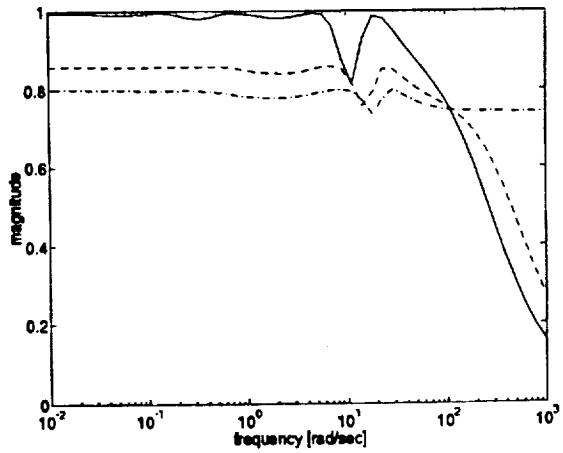


Figure 7: Robust performance bounds for uncertainty in $\alpha$: case 1 (dash dot), case 2 (dash), case 3 (solid).

| case | frequencies (rad/sec) | % of unheated frequencies | cover function | | |
|---|---|---|---|---|---|
| | | | $k_c$ | $\zeta_c$ | $\omega_c$ |
| 1 | 18.53, 35.34, 48.63 | 100% | 2.5 | 0.25 | 19.53 |
| 2 | 14.82, 28.27, 38.91 | 80% | 3 | 0.25 | 15.82 |
| 3 | 11.12, 21.20, 29.18 | 60% | 3 | 0.2 | 11.12 |

Table 1: Uncertainty levels in $\alpha$.

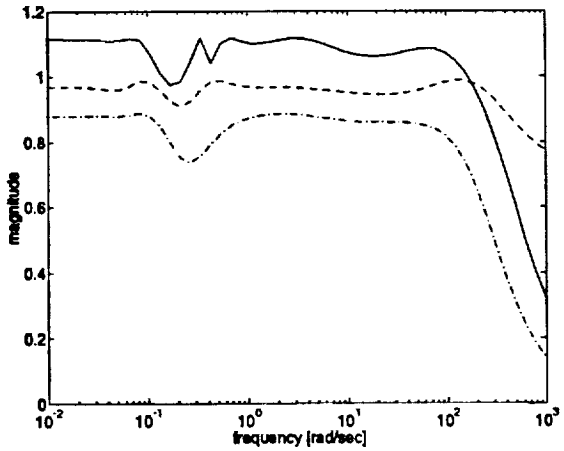


Figure 8: Robust performance bounds for 10% (dash dot), 20% (dash) and 30% (solid) in the actuators.

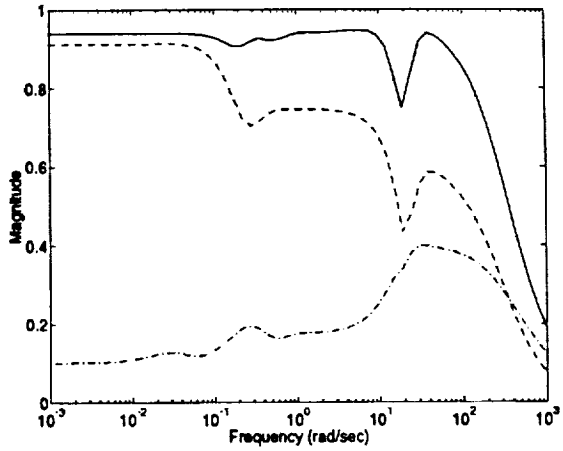


Figure 9: Robust performance (solid), nominal performance (dash) and robust stability (dash dot) for a $\mu$ design including all uncertainties.

achievable at the 30% level. The simultaneous presence of two uncertainties clearly reduces the level of obtainable robust performance. However, it should be noted that uncertainty in controlling thrust may be less than that for controlling pitching moment.

The sensitivity studies indicate that uncertainty in $c_{M\alpha}$ is not as critical as uncertainty in $\alpha$ or in the control effectiveness. The effect of propulsion system variations on the pitching moment due to angle of attack changes of the rigid body are not potentially "dangerous" for the stability of the vehicle. Flexible fuselage bending becomes more important the closer the elastic frequencies get to the rigid body frequencies. Uncertainty in the control effectiveness is also crucial for higher uncertainty levels at low frequencies. These results illustrate the trends when the uncertain effects appear one at a time. A design allowing for mutual coupling is investigated in the following section.

### 6. Design for Robust Performance

A $\mu$-controller for all types of uncertainty being present simultaneously was designed. The results of a design with 25% uncertainty in $c_{M\alpha}$, uncertainty in the angle of attack corresponding to case 1 in Table 1, and 10% uncertainty in the actuators are illustrated in Fig. 9. Robust performance is achieved at all frequencies. The time responses for the nominal model with no uncertainty for simultaneous step commands in velocity ($V_c$ = 100 ft/sec) and altitude ($h_c$ = 1000 ft) while encountering longitudinal and vertical atmospheric turbulence are shown in Figs. 10-15. Velocity and altitude responses compare well with the $H_\infty$ design for the nominal model (Figs. 10 and 11). Both meet the performance requirements. The altitude curve exhibits a little 'dip' towards the end which is due to influence of turbulence. The magnitudes of the variations in angle of attack, normal acceleration, elevon deflection and fuel flow are reasonable considering the level of turbulence present in the simulation. Figs. 12-15 illustrate the effect of turbulence on the system.

Fig. 13 shows that turbulence causes a $\pm$0.05g variation in the normal acceleration sensed by the pilot. This can be reduced by penalizing $n_z$ in the design at the expense of increasing the bandwidth of the pitch loop and increasing the coupling with the flexible mode.

The singular values of the loop transfer function with the loop broken where velocity and altitude are fedback to the controller are shown in Fig. 16, for both the $H_\infty$ and the $\mu$ design. The bandwidth of the $\mu$-synthesis design is reduced and the crossover freequencies of the minimum and maximum singular values are closer together.

Figs. 17 and 18 compare the time responses of a

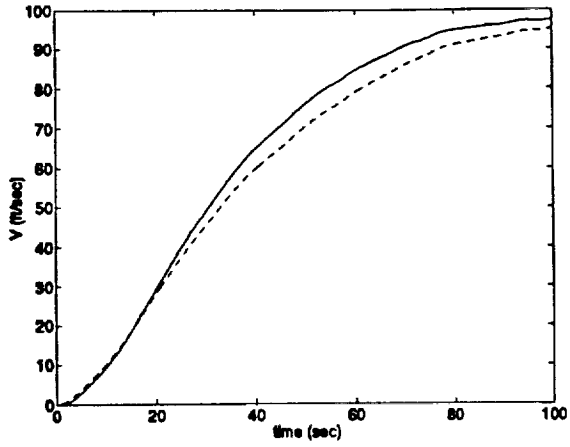


Figure 10: Velocity response for nominal performance, $H_\infty$ design (solid), $\mu$ design (dash).

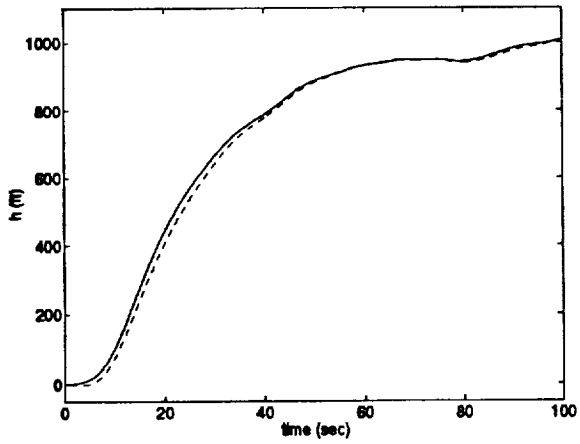


Figure 11: Altitude response for nominal performance, $H_\infty$ design (solid), $\mu$ design (dash).

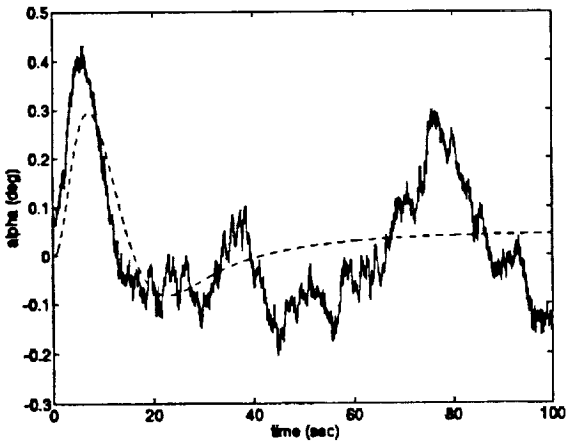


Figure 12: Angle of attack response for $\mu$ design, with (solid) and without (dash) turbulence.

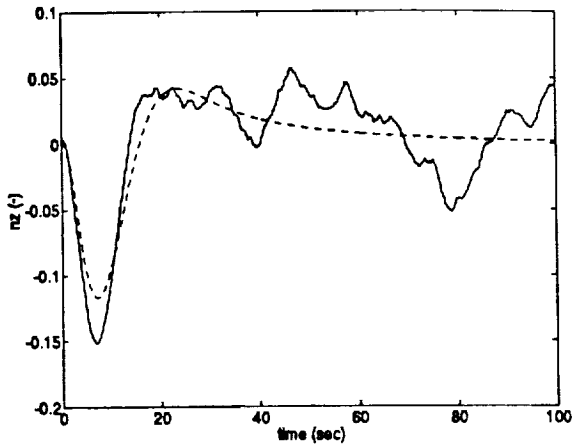


Figure 13: Normal acceleration response for $\mu$ design, with (solid) and without (dash) turbulence.

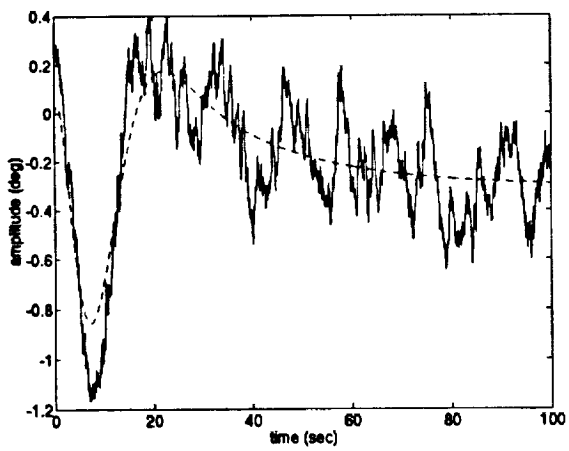


Figure 14: Elevon response for $\mu$ design, with (solid) and without (dash) turbulence.

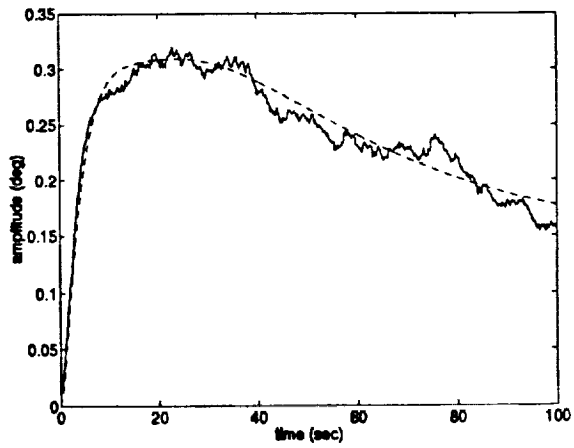


Figure 15: Fuel equivalence ratio response for $\mu$ design, with (solid) and without (dash) turbulence.

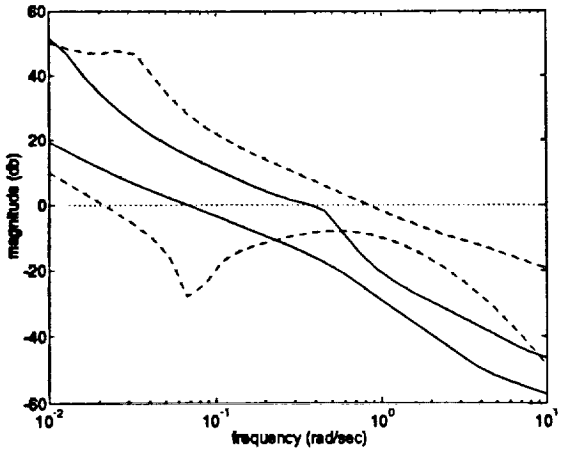


Figure 16: Singular value plots for loop broken at V and h feedback, $H_\infty$ design (dash), $\mu$ design (solid).

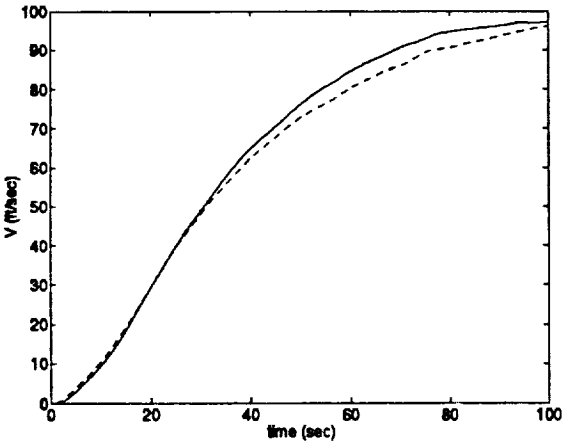


Figure 17: Velocity responses for $H_\infty$ design (solid) and perturbed $\mu$ design (dash).

perturbed system using the $\mu$-controller to the nominal response of the $H_\infty$ design. The perturbations that are introduced into the system were chosen to be the worst case and of the same magnitude as those for which the $\mu$-controller was designed. Figs. 17 and 18 illustrate that $H_\infty$ performance can be maintained by a $\mu$-controller for a system with four simultaneous perturbations.

The effects of the uncertainties cannot be considered seperately. Uncertainty in control effectiveness changes the elevon deflections affecting the angle of attack changes due to flexible body bending. This variation in $\alpha$ adds to the rigid body angle of attack which again influences the impact of the propulsion system on the pitching moment. Obviously, coupling between the individual effects occurs affecting and possibly amplifying the uncertain characteristics. When a controller design for higher levels of uncertainty is performed, robust performance cannot be achieved (see Fig. 19). 100% uncertainty in $c_{M\alpha}$, uncertainty in $\alpha$ correponding to case 3 in Table 1 and 20% uncertainty in control effectiveness were used.

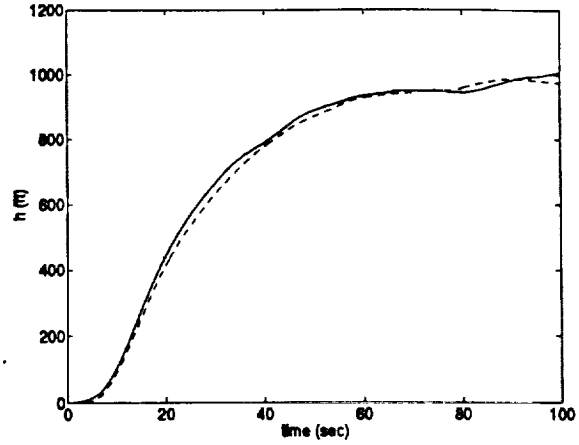


Figure 18: Altitude responses for $H_\infty$ design (solid) and perturbed $\mu$ design (dash).

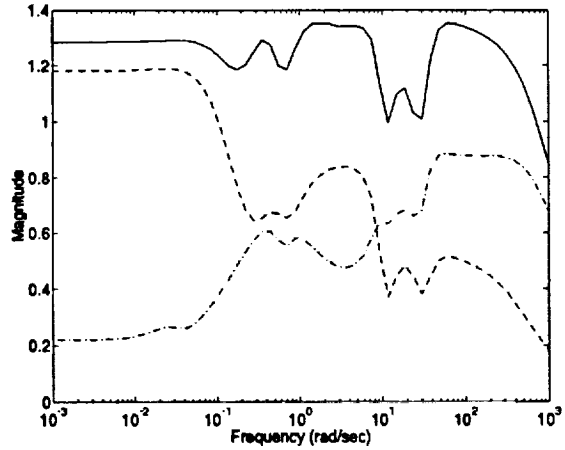


Figure 19: Robust performance (solid), nominal performance (dash) and robust stability (dash dot) for a $\mu$ design with increased uncertainty levels.

These values allowed robust performance in the individual designs. Still, with a maximum value of the robust performance bound at around 1.35, the result is not "devastating". Robust stability is maintained.

## 7. Controller Order Reduction

The order of the $\mu$-controller accounting for all uncertainties is 38. The vehicle was represented by a five state longitudinal model, and the generalized plant including all frequency dependent weights for performance and uncertainty is $16^{th}$ order. Designing for robust performance considering structured uncertainty (D scaling) increased the order of the controller considerably. When implemented, large order controllers can create time delays which may be undesirable. One solution to this problem is to use model order reduction on the controller realization. This method, though, does not consider the properties of the closed loop system when reducing the order of the controller, i.e. robustness properties are not guaranteed.

To investigate this issue, an order reduction of the

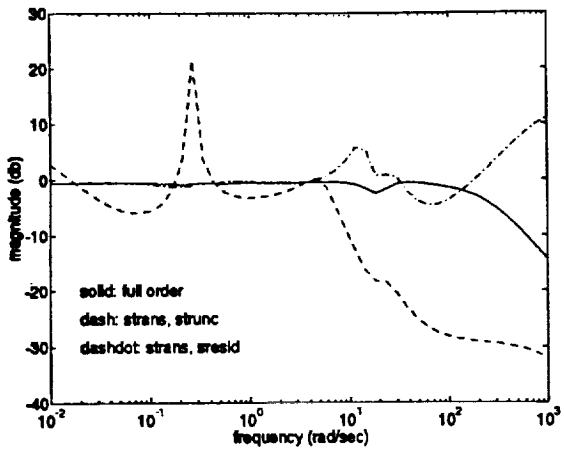


Figure 20: Robust performance bounds for 26 state reduced order controllers.

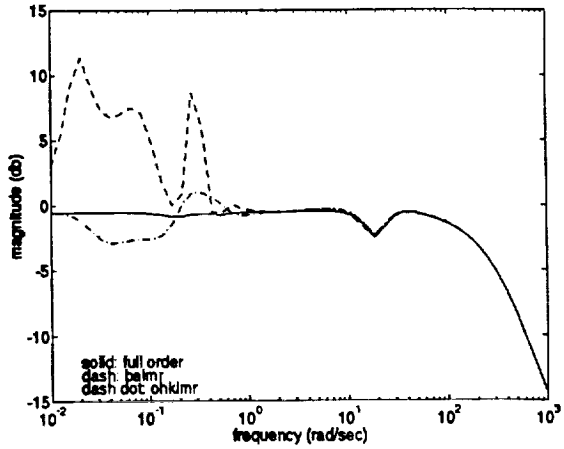


Figure 21: Robust performance bounds for 20 state reduced order controllers.

controller was performed using several different methods provided by the MATLAB toolboxes *μ-TOOLS* [14] and *Robust Control Toolbox* [15]. Not all methods could be applied since the controller is unstable. In a first step, the order of the controller was reduced by 12 resulting in a 26 state controller. Robust performance bounds are illustrated in Fig. 20,which clearly demonstrates that robust performance of the full order controller is not maintained. The methods displayed in Fig. 20 are truncating (*strunc*) and residualizing (*sresid*) a controller which has been transformed to bidiagonal form (*strans*) Ref. [14]. The other methods utilized in this comparison are a balanced model reduction (*balmr*) and an optimal Hankel approximation (*ohkl*) from Ref. [15]. Both preserved robust performance for the 26 state controller (not shown) but lost this property when the controller order was chosen to be 20, (see Fig. 21).

Another approach to design low order compensators is to constrain the order of the controller in the design process, and promising results have been achieved in Refs. [16] and [17]. This technique combined with the framework of $\mu$ synthesis will be addressed in future research.

## 8. Conclusions

A control study of an hypersonic vehicle with air-breathing propulsion has been performed in this paper. Special consideration is given to modeling the uncertainty due to propulsive and aeroelastic effects and control effectiveness. The impact on achievable robust performance was examined. A sensitivity study of robust performance achievable with various levels of uncertainty shows that flexible fuselage bending and uncertainty in control effectiveness have a greater impact on achievable robust performance than propulsion system variations due to angle of attack changes. A design example for robust performance illustrated that $H_\infty$ and $\mu$-synthesis is ideal for addressing the problem of multiple uncertainty sources present in flight control systems. Acceptable uncertainty levels degrade when all uncertainties occur simultaneously. This implies that uncertainty modeling will play a crucial role in successful flight control system design for hypersonic vehicles.

An order reduction of the resulting controller discloses that robust performance is not guaranteed for the reduced order system. Future research will focus on fixed order controller design and the issue of treating real parameter uncertainty.

## Acknowledgments

This research is supported by NASA's Langley Research Center under grant NAG-1-1451. Mr. John D. McMinn and Ms. Irene M. Gregory are the technical monitors.

## References

[1] Schmidt, D.K., Mamich, H. and Chavez, F., "Dynamics and Control of Hypersonic Vehicles - The Integration Challenge For the 1990's," AIAA-91-5057, AIAA $3^{rd}$ International Aerospace Planes Conference, Orlando, FL, December 1991.

[2] Calise, A.J. and Buschek, H., "Research in Robust Control for Hypersonic Vehicles," Progress Report No. 1 to NASA Langley Research Center, Contract No. NAG-1-1451, November 1992.

[3] Raney, D.L. et al, "Impact of Aeroelasticity on Propulsion and Longitudinal Flight Dynamics of an Air-Breathing Hypersonic Vehicle," AIAA-93-1367, $34^{th}$ Structures, Structural Dynamics and Materials Conference, La Jolla, CA, April 1993.

[4] Doyle, J.C. et al, "State-Space Solutions to Standard $H_2$ and $H_\infty$ Control Problems," IEEE

Transactions on Automatic Control. Vol. 34, No. 8, August 1989, pp. 831-846.

[5] Doyle, J.C., Wall, J.E. and Stein, G., "Performance Robustness Analysis for Structured Uncertainty," Proceedings of the 21$^{st}$ IEEE Conference on Decision and Control, Orlando, FL, December 1982, pp. 629-636.

[6] Doyle, J.C., "Structured Uncertainty in Control System Design," Proceedings of the 24$^{th}$ IEEE Conference on Decision and Control, Ft. Lauterdale, FL, December 1985, pp. 260-265.

[7] Shaughnessy, J.D. et al, "Hypersonic Vehicle Simulation Model: Winged-Cone Configuration," NASA TM 102610, November 1990.

[8] Gregory, I.M., McMinn, J.D., Shaughnessy, J.D. and Chowdhry, R.S., "Hypersonic Vehicle Control Law Development Using $H_\infty$ and $\mu$-Synthesis," Presented at the 4$^{th}$ AIAA International Aerospace Planes Conference, Orlando, FL, December 1992.

[9] Turner, R.E. and Hill, C.K., "Terrestrial Environment (Climatic) Criteria Guidelines for Use in Aerospace Vehicle Development, 1982 Revision," NASA TM 82473, June 1982.

[10] Justus, C.G. et al, "New Atmospheric Turbulence Model for Shuttle Applications," NASA TM 4168, January 1990.

[11] Walton, J., "Performance Sensitvity of Hypersonic Vehicles to Changes in Angle of Attack and Dynamic Pressure," AIAA-89-2463, 25$^{th}$ Joint Propulsion Conference, Monterey, CA, July 1989.

[12] Paz, M., "Structural Dynamics, Theory and Computation," 3$^{rd}$ edition, van Nostrand Reinhold, New York, 1991.

[13] Heeg, J. et al, "Aerothermoelastic Analysis of a NASP Demonstrator Model," AIAA-93-1366, 34$^{th}$ Structures, Structural Dynamics and Materials Conference, La Jolla, CA, April 1993.

[14] Balas, G.J. et al, "$\mu$-Analysis and Synthesis Toolbox, User's Guide," The MathWorks Inc., Natick, MA, April 1991.

[15] Chiang, R.Y. and Safonov, M.G., "Robust Control Toolbox, User's Guide," The MathWorks Inc., Natick, MA, August 1992.

[16] Byrns, E.V. Jr. and Calise, A.J., "Approximate Recovery of $H_\infty$ Loop Shapes Using Fixed Order Dynamic Compensation," AIAA-91-2729, AIAA Guidance, Navigation and Control Conference, New Orleans, LA, August 1991.

[17] Sweriduk, G.D. and Calise, A.J., "Robust Fixed Order Dynamic Compensation: A Differential Game Approach," 1993 IEEE Conference on Aerospace Control Systems, West Lake Village, CA, May 1993.

## Appendix

The effect of turbulence on the system is modeled by

$$\dot{x} = Ax + Bu + B_g \begin{bmatrix} V_g \\ \alpha_g \\ q_g \end{bmatrix}$$

where

$$B_g = \begin{bmatrix} -a_{11} & -a_{12} & 0 \\ -a_{21} & -a_{22} & 0 \\ -a_{31} & -a_{32} & -a_{33} \\ 0 & 0 & 0 \\ 0 & 0 & 0 \end{bmatrix}$$

The elements in $B_g$ are the corresponding elements of the $A$ matrix. The pitch rate due to gust $q_g$ can be expressed in terms of the angle of attack rate

$$q_g = -\frac{\dot{w}_g}{V_0} = -\dot{\alpha}_g$$

The numerical values for the $A$ and $B$ matrices are given by

$$A = \begin{bmatrix} 3.6524 \cdot 10^{-3} & -9.6679 \cdot 10^{-1} & 0 & -5.5639 \cdot 10^{-1} & -1.4321 \cdot 10^{-3} \\ -3.9195 \cdot 10^{-5} & -8.1626 \cdot 10^{-2} & 1 & -8.4420 \cdot 10^{-5} & 9.2560 \cdot 10^{-6} \\ 2.0147 \cdot 10^{-3} & 3.0354 & -9.5218 \cdot 10^{-2} & 1.5500 \cdot 10^{-5} & -1.0766 \cdot 10^{-5} \\ 2.7263 \cdot 10^{-6} & 7.7679 \cdot 10^{-6} & 1 & -7.7679 \cdot 10^{-6} & -1.0188 \cdot 10^{-9} \\ 2.0779 \cdot 10^{-2} & -1.3701 \cdot 10^{2} & 0 & 1.3701 \cdot 10^{2} & 0 \end{bmatrix}$$

$$B = \begin{bmatrix} 9.6995 \cdot 10^{-2} & 7.5989 \\ 3.3486 \cdot 10^{-3} & -2.0942 \cdot 10^{-3} \\ 1.0825 & 0 \\ 0 & 0 \\ 0 & 0 \end{bmatrix}.$$